Multiple-quantum spin coherence in the ground state of alkali atomic vapors

J. D. Xu, G. Wäckerle, and M. Mehring
2. Physikalisches Institut, Universität Stuttgart, D-70550 Stuttgart, Germany
(Received 24 May 1996)

Two-dimensional (2D) multiple-quantum coherence is reported for the hyperfine ground state of rubidium and cesium atoms by applying multiple radio-frequency pulses to the optically polarized atoms. Calculations of 1D and 2D multiple quantum coherences were performed with a general theory for an arbitrary high spin system by using irreducible tensor operators. The experimental results compare very well with the calculations. [S1050-2947(97)06001-0]

PACS number(s): 32.30.Dx, 32.60.+i, 32.80.Bx, 32.80.Wr

I. INTRODUCTION

Multiple-quantum (MQ) coherences are an important branch in magnetic resonance [1–3], and are widely applied in nuclear magnetic resonance (NMR) [4]. Although first observed and discussed in optical spectroscopy [5], multiple-quantum spectra are rarely observed in optically detected magnetic resonance (ODMR) and a few publications deal with continuous wave multiple-quantum spectra [6,7]. Using multiple radio-frequency pulse techniques different kinds of MQ techniques have been developed, especially in the field of NMR. But most of the work deals with multilevel systems derived from the coupling of many spin-1/2 particles [8,9]. Rather few publications have dealt with spin $I>1/2$ systems [1,10–12].

Here we report on radio-frequency (rf) and optical double resonance experiments by applying circular polarized light parallel to a magnetic field B_0 in order to optically pump [13] the alkali atoms (rubidium and cesium) in the ground state, characterized by the total angular momentum quantum number F. For magnetic fields in the range of 1 mT the linear and quadratic Zeeman interaction leads to a level splitting into unequally spaced Zeeman sublevels labeled by the magnetic quantum number M_F. Magnetic dipole transitions ($\Delta M_F=\pm 1$) can be induced by rf pulses creating oscillating magnetic fields perpendicular to the static B_0 field direction. We have applied the standard three-pulse sequence in order to create multiple-quantum coherences (with $1\leqslant\Delta M_F\leqslant F$) which were detected optically.

Certainly the ground state of the alkali atoms has been investigated very intensively and no new physics is expected to arise. However, the unique high spin quantum numbers of these states in conjunction with the quadratic Zeeman effect provides an ideal playground for quantum coherence experiments. In fact, equivalent multilevel systems are not available from nuclear spin states alone. Although high spin states of a few nuclei exist, the appropriate quadrupole interaction must be present, which requires just the right nuclear quadrupole moment, electric field gradient, and atomic site within a single crystal in order to set up a level splitting which can be covered by the available rf fields. These favorable conditions are rarely found in real physical systems. In the alkali atoms the splitting can be adjusted by the magnetic field and the sample preparation is simple. We have therefore chosen these systems to demonstrate different variants of multiple-quantum coherence in atomic vapors, the results of which likely come as a surprise to the nonexpert reader. Moreover, from a theoretical point of view these spin systems are simple enough to be treated rigorously, but complicated enough to be nontrivial.

We recall that the ground state effective spin quantum numbers F are $F=1,2$, $F=2,3$, and $F=3,4$ for ^{87}Rb, ^{85}Rb, and ^{133}Cs, respectively. One possibility would be to treat these multilevel systems by two-level or fictitious spin-1/2 operators [1]. We prefer here, however, to use irreducible tensors [14]. The irreducible tensor operator T_{kq} displays directly the physical properties with $q=\Delta M_F=0,\pm 1,\ldots,\pm k$ being the multiquantum order, and where k is the rank of the tensor and the upper limit for the quantum order q.

In this paper we derive a general theory for multiple-quantum coherences for large integer spins F and discuss the principle of creation and detection of multiple-quantum coherences with a series of three rf pulses in Sec. II. We present the experimental arrangement, the method, and results of one-dimensional (1D) multiple-quantum spectra with large and small frequency offsets in Sec. III. In Sec. IV we discuss the experimental technique and the results of two-dimensional MQ spectra and compare them with calculated 2D MQ spectra obtained from irreducible tensor calculations.

II. THE PRINCIPLE OF MULTIPLE-QUANTUM SPIN COHERENCE IN ATOMS

In this section we address two points, namely, (i) what we mean by multiple-quantum coherence in atoms, and (ii) how it can be created and detected.

MQ coherence can only be excited in multilevel systems, for example, due to the coupling of many spin-1/2 or by uncoupled high spin-F systems. In this paper we only discuss the second case.

To be more specific we show in Fig. 1 an alkali atom ground state with $F=3$ (e.g., cesium) which is split into seven sublevels in a magnetic field. In a one-quantum (1Q) process the atom transits from sublevel M_F to sublevel $M_F\pm 1$ with the difference in quantum number between neighboring sublevels being $\Delta M_F=\pm 1$. When the magnetic field is small, only a single line is observed. With increasing magnetic field, a nonlinear term (proportional to M_F^2, the

 © 1997 The American Physical Society

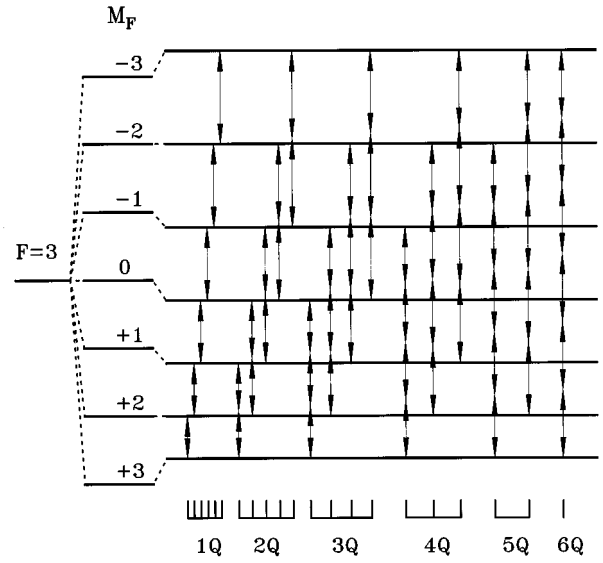

FIG. 1. Zeeman level scheme of an alkali $F=3$ ground-state hyperfine multiplet showing the contributions of linear and quadratic Zeeman interactions separately. All possible n-quantum transitions (nQ with $n=1,\ldots,6$) are indicated by the arrows.

quadratic Zeeman interaction) appears, which can be described by a pseudoquadrupole operator together with a characteristic frequency ν_Q, and which shifts the Zeeman sublevels, leading to a multiline spectrum. For $F=3$ (see Fig. 1) six lines will be observed in the 1Q spectrum and the difference frequency between neighboring lines is $2\nu_Q$. In a two-quantum process the atomic state shifts from sublevel M_F to $M_F\pm 2$ while absorbing or emitting two quanta of energy. For $F=3$, this will lead to a five line 2Q spectrum. The frequency difference between these lines is $4\nu_Q$. The other three-, four-, five-, and six-quantum processes may be deduced in a similar way. The corresponding 3Q, 4Q, 5Q, and 6Q spectrum consist of four, three, two, and one line, respectively. For an $F=3$ system Fig. 1 displays all possible nQ transitions indicated by the arrows. The corresponding nQ spectra are shown schematically as stick diagrams at the bottom.

A. Basic properties of rf operators and the system Hamiltonian

Before we discuss multiple-quantum processes, we will briefly explain the role of the radio-frequency pulse and the system Hamiltonian in the evolution process. The spin density matrix can be conveniently expressed by irreducible tensor operators (T_{kq}) as

$$\rho=\sum_{k,q}\langle T_{kq}^{\dagger}\rangle T_{kq}, \tag{1}$$

where $\langle T_{kq}^{\dagger}\rangle$ is a multipole expectation value of rank k and quantum number q with $k=0,\ldots,2F$, and $-k\leqslant q\leqslant k$. We choose the z axis parallel to the magnetic field B_0, as the quantization axis and apply rf pulses along the y axis of the rotating frame. The rotation operator for the pulse can be expressed as usual by $U_y=\exp(i\beta I_y)$, where $\beta=\omega_1 t$ is the pulse rotation angle, ω_1 is the Rabi precession frequency, and where $I_y=i(T_{11}+T_{1-1})/\sqrt{2}$. The density matrix after the rf pulse can be expressed as [12]

$$\rho_1=U_y^{\dagger}\rho U_y=\sum_{k,q}\langle T_{kq}^{\dagger}\rangle U_y^{\dagger}T_{kq}U_y=\sum_{k,q,q'}\langle T_{kq}^{\dagger}\rangle d_{q'q}^{k}(\beta)T_{kq'}, \tag{2}$$

where the $d_{q'q}^{k}(\beta)$ are the Wigner rotation matrices. From this it is obvious that the rf pulse changes only the quantum number q of the tensor operator T_{kq} and keeps the rank k unchanged. This is an important property of the rf pulse which will be utilized in the next section to create MQ coherence.

The system Hamiltonian can be split into two parts, namely, a linear and a nonlinear term,

$$H=H_0+H_Q=\hbar\omega_F T_{10}+\sqrt{\frac{2}{3}}\hbar\omega_Q T_{20}, \tag{3}$$

where ω_F is the Larmor frequency and ω_Q is a pseudoquadrupolar frequency reflecting the quadratic Zeeman interaction. By making an expansion of the Breit-Rabi [15] expression up to terms proportional to M_F^2 one deduces the relation

$$\omega_Q=\mp\frac{2\pi\nu_0 x^2}{(2I+1)^2}\sqrt{\frac{(2F+3)(2F+1)F(2F-1)(F+1)}{30}}, \tag{4}$$

with

$$x=\frac{(g_J-g_I')\mu_B B_0}{h\nu_0}\quad\text{and}\quad F=I\pm\frac{1}{2},$$

where ν_0 is the frequency splitting between the two hyperfine multiplets in the ground state of the alkali-metal atoms, g_J and g_I' are the electron Landé factors for total angular moment J and nuclear g factor, respectively. The Bohr magneton is denoted by μ_B and B_0 is the applied magnetic field. The $\pm$ and $\mp$ signs correspond to the two hyperfine levels in the alkali ground state ($F=I\pm\frac{1}{2}$).

For further use we define the following symmetric and antisymmetric tensor operators,

$$T(s)_{kq}=\frac{1}{\sqrt{2}}(T_{kq}+T_{k-q}),$$

$$T(a)_{kq}=\frac{1}{\sqrt{2}}(T_{kq}-T_{k-q}). \tag{5}$$

This will simplify the following expressions considerably. The effect of the linear Zeeman term on the spin density matrix is given by the evolution operator $U_Z(t)=\exp(iH_0t/\hbar)$. Its effect on the symmetric and antisymmetric tensor operators $T(s)_{kq}$ and $T(a)_{kq}$ is readily calculated as [11]

$$U_Z(t)^{\dagger}T(s)_{kq}U_Z(t)=T(s)_{kq}\cos(q\omega_F t)-iT(a)_{kq}\sin(q\omega_F t),$$

$$U_Z(t)^{\dagger}T(a)_{kq}U_Z(t)=T(a)_{kq}\cos(q\omega_F t)-iT(s)_{kq}\sin(q\omega_F t). \tag{6}$$

It is clear from these expressions that the linear Zeeman operator neither changes the rank k nor the quantum number q of the tensor operators, it merely converts the symmetric tensor operator into the antisymmetric tensor operator and vice versa.

The evolution operator of the pseudoquadrupolar term $U_Q(t)=\exp(iH_Q t/\hbar)$, however, leads to more complex expressions. It is not possible to derive a general simple form for arbitrary quantum number. We therefore represent the case $F=1$ as a special example [11]:

$$
\begin{aligned}
U_Q^\dagger(t)T(s)_{11}U_Q(t)&=T(s)_{11}\cos\omega_Q t-iT(a)_{21}\sqrt{2}\sin\omega_Q t,\\
U_Q^\dagger(t)T(a)_{11}U_Q(t)&=T(a)_{11}\cos\omega_Q t-iT(s)_{21}\sqrt{2}\sin\omega_Q t,\\
U_Q^\dagger(t)T(s)_{21}U_Q(t)&=T(s)_{21}\cos\omega_Q t-iT(a)_{11}\frac{1}{\sqrt{2}}\sin\omega_Q t,\\
U_Q^\dagger(t)T(a)_{21}U_Q(t)&=T(a)_{21}\cos\omega_Q t-iT(s)_{11}\frac{1}{\sqrt{2}}\sin\omega_Q t.
\end{aligned}
\tag{7}
$$

All other tensor operators like T_{10}, T_{20}, $T(s)_{22}$, and $T(a)_{22}$, which do not appear in Eqs. (7), commute with the Hamiltonian H_Q. We observe in Eqs. (7) that $U_Q(t)$ only changes the symmetry and rank k of the $k1$ components of the tensor operators and keeps the quantum number $q=1$ constant. This is just the opposite effect as compared with the operation of the rf pulse. By combining these mutually opposite effects, one can create MQ coherence.

With the detection scheme applied in our experiments we are limited to observe $\langle T(s)_{11}^\dagger\rangle$ only. Our optically detected signal S can therefore be expressed [16] as

$$
S=-i\frac{\sqrt{2}}{4}\sum_{F_e} VC_1\langle T(s)_{11}^\dagger\rangle, \tag{8}
$$

with

$$
V=-\frac{\omega_l\ell}{2\hbar\varepsilon_0 c}\int_{-\infty}^{+\infty}\frac{(\omega_l-\omega_0-\mathbf{k}\cdot\mathbf{v})f(\mathbf{v})d\mathbf{v}}{(\omega_l-\omega_0-\mathbf{k}\cdot\mathbf{v})^2+\Gamma^2/4}
$$

and

$$
C_1=(-1)^{F_g+F_e}d_{F_eF_g}d^*_{F_eF_g}\begin{Bmatrix}1 & 1 & 1\\ F_g & F_g & F_e\end{Bmatrix},
$$

where ω_l is the laser frequency, ω_0 is the atomic transition frequency from the ground state F_g to the excited state F_e, $\mathbf{v}$ is the velocity of the atoms, $f(\mathbf{v})$ is the Maxwell-Boltzmann velocity distribution, and ℓ is the optical length of the sample. The other parameters are the half-width Γ of the optical absorption line, the dielectric constant ε_0, the transition probability $d_{F_eF_g}$, and C_1 is a constant for a given optical hyperfine transition. The dispersion line shape function V is antisymmetric with respect to the atomic optical resonance frequency ω_0. The most important term $\langle T(s)_{11}^\dagger\rangle$ which is a multipole of rank 1 and quantum number 1 contains the information on the spin system. Any MQ coherence must therefore be transferred into this multipole order before it can be detected.

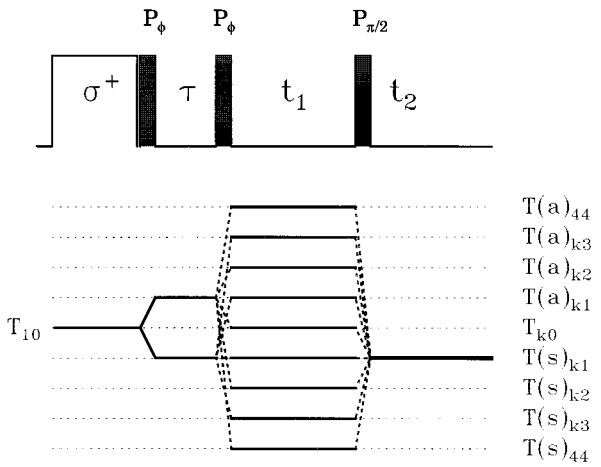

FIG. 2. Pulse sequence (top) for creation and detection of multiple-quantum coherence. Initially the atoms are optically pumped by a circularly polarized optical pulse, then a sequence of three rf pulses follows. The evolution of the tensor components under the action of the rf pulses and the system Hamiltonian is depicted symbolically on the bottom (for details see text).

B. Creation and detection of MQ coherence

The rf-pulse sequence used for MQ-coherence experiments is quite standard and is shown in Fig. 2. It can be separated into three parts, (a) the spin polarization of the atom in B_0 direction by optical pumping through laser light of σ^+ polarization, (b) application of a rf $(\pi/2)_\phi$ pulse pair for creating MQ coherence and evolution of the multipoles during time t_1, and (c) application of a third rf $(\pi/2)$ pulse combined with a delay $t_2=\tau$ after which optical detection occurs for transfer of the higher-quantum multipoles $\langle T_{kq}^\dagger\rangle$ to the detection multipole $\langle T(s)_{11}^\dagger\rangle$.

The circularly polarized pumping light propagates along the direction of the magnetic field B_0 and spin polarizes the atoms along the B_0 direction. In the high temperature approximation under weak pumping conditions the density matrix can be expressed as $\rho(0)=\langle T_{10}^\dagger\rangle T_{10}$. The first $(\pi/2)_\phi$ rf pulse creates a coherent multipole which can be expressed in terms of the symmetric $\langle T(s)_{11}^\dagger\rangle$ and antisymmetric $\langle T(a)_{11}^\dagger\rangle$ multipole as discussed before. After an evolution for a time τ, the pseudoquadrupole term transforms the rank of these tensor components which keep the quantum number q of the tensor operators constant. In other words, $\langle T(s)_{11}^\dagger\rangle$ and $\langle T(a)_{11}^\dagger\rangle$ are transformed into $\langle T(s)_{k1}^\dagger\rangle$ and $\langle T(a)_{k1}^\dagger\rangle$ with $k=1,\ldots,2F$. The second $(\pi/2)_\phi$ rf pulse increases the quantum number q for each component, that is, $\langle T(s)_{k1}^\dagger\rangle\rightarrow\langle T(s)_{kq}^\dagger\rangle$ with $q=0,\ldots,k$. During evolution time t_1, the pseudoquadrupole term mixes the different ranks of the tensor operators $T(s,a)_{kq}$ while keeping the corresponding quantum number q constant. The third $(\pi/2)$ rf pulse can be visualized as a readout pulse. It mixes different quantum numbers q of the multipole $\langle T_{kq}^\dagger\rangle$ and transfers them into the single-quantum detection multipole $\langle T(s)_{11}^\dagger\rangle$.

These processes are sketched in the lower part of Fig. 2. Every horizontal line represents tensor operators T_{kq} with the same quantum number q. When the trajectory changes to a different horizontal line, it implies that the quantum number q has been changed.

After some algebra, we can express the detection multipole in the following form:

$$\langle T(s)^{\dagger}_{11}\rangle = T_{S_0}(\phi,\tau,t_2) + T_{S_1}(\phi,\tau,t_1,t_2), \tag{9}$$

where

$$T_{S_0}(\phi,\tau,t_2) = i\cos(\omega_F\tau)\sin(\omega_F t_2) M_{CPPC}(11,11),$$

$$T_{S_1}(\phi,\tau,t_1,t_2) = i[\cos(\omega_F\tau)\sin(\omega_F t_2) M_{CPCPC}(gc,11) + \sin(\omega_F\tau)\cos(\omega_F t_2) M_{CPCPC}(uc,11)], \tag{10}$$

and

$$M_{CPCPC}(mn,kq) = \sum_{j=q}^{4} M_{CPCP}(mn,jq) C^{jq}_{kq},$$

$$M_{CPPC}(11,kq) = \sum_{j=(q-1)/2}^{1} M_{CP}(11,2j+1;0) \times P^{2j+1,0}_{2j+1,1} C^{2j+1,1}_{kq},$$

$$M_{CPCP}(uc,kq) = \sum_{j=0}^{j=1(k\geq 3)} M_{CPC}(11,k2j+1) \times P^{k,2j+1}_{kq} \cos[(2j+1)y], \tag{11}$$

$$M_{CPCP}(gs,kq) = \sum_{j=1}^{j=2(k\geq 3)} M_{CPC}(11,k2j) P^{k,2j}_{kq} \sin 2jy,$$

$$M_{CP}(11,kq) = C^{11}_{k1} P^{k,1}_{kq},$$

$$M_{CPC}(11,kq) = \sum_{j=q}^{4} M_{CP}(11,jq) C^{jq}_{kq}.$$

Here, ω_F is the Larmor frequency, and the symbol mn in the coefficients $M_{CPCPC}(mn,11)$ represents either gc, uc, gs, or us. The symbols gc and uc are short forms for cosine function with even and odd multiples of the fundamental frequency $y=\omega_F t_1+\phi$, that is, terms of the form $\cos(2jy)$, $\cos[(2j+1)y]$ with integer j. The symbols gs and us represent the corresponding sine function with even and odd multiples of the fundamental frequency y, that is, terms of the form $\sin(2jy)$, $\sin[(2j+1)y]$ with integer j. The coefficients $M_{CPCPC}(mn,11)$, $M_{CPCPC}(gc,11)$, and $M_{CPCPC}(uc,11)$ describe the multipole transfer by three rf pulses in combination with the pseudoquadrupole Hamilton operator. The subscript of the coefficients M is a combination of the two letters C and P, where C and P label the corresponding operations by the pseudoquadrupole operator and the rf pulse, respectively. The coefficients $P^{n_1,n_2}_{n_3,n_4}$ and $C^{m_1,m_2}_{m_3,m_4}$ are tabulated in Ref. [17] up to rank $k=6$. The detection multipole $\langle T(s)^{\dagger}_{11}\rangle$ consists of two parts, namely, the $T_{S_0}(\phi,\tau,t_2)$ part which is independent of time t_1, and another term $T_{S_1}(\phi,\tau,t_1,t_2)$ which depends on t_1. In our measurements we set $t_2=\tau$. The optically detected 1D signal can now be expressed in the following way:

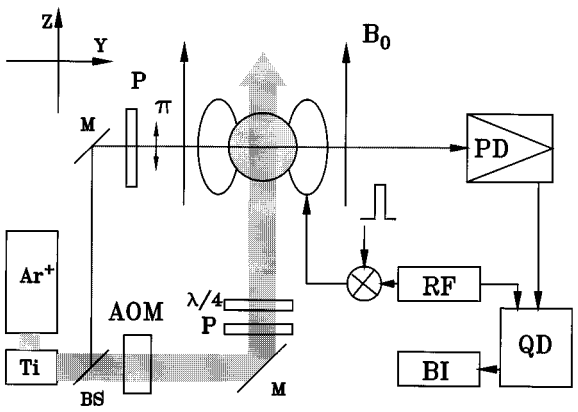

FIG. 3. Experimental arrangement for multiple-quantum spectroscopy of optically pumped alkali vapors. (Ar^+: argon-ion laser, Ti: titanium-sapphire laser, BS: beam splitter, AOM: acousto-optic modulator, P: polarizer, λ/4: quarter-wave plate, M: mirror, PD: polarimeter detector, QD: quadrature detector, BI: gated boxcar integrator, RF: rf synthesizer).

$$S_{1D}(t_1) = \sum_{F_g,F_e} -\frac{\sqrt{2}}{4} iVC_1[T_{S_1}(\tau,t_1,\tau)e^{-(2\tau+t_1)/T_2} + T_{S_0}(\tau,\tau)e^{-2\tau/T_2}]. \tag{12}$$

After Fourier transformation we obtain a 1D MQ spectrum.

$$F_{1D}(\omega) = \int_0^{\infty} dt_1 \exp(-i\omega t_1) S_{1D}(t_1). \tag{13}$$

According to Eq. (13) we can calculate any 1D MQ spectrum for arbitrary spin F, where for different spins F the coefficients in the terms T_{S_1} and T_{S_0} will be different.

III. ONE-DIMENSIONAL MULTIPLE-QUANTUM SPECTRA

A. Experimental arrangement

The experiments were performed only on one of the two ground state hyperfine level systems of rubidium or cesium atoms. For ^{87}Rb this is $F=2$, for ^{85}Rb it is $F=3$, and for ^{133}Cs we used the $F=4$ manifold. These alkali metals were sealed in a 2 cm^3 glass sphere including some mbar of nitrogen as a buffer gas to increase spin-relaxation times. The number density of the alkali atoms was controlled by a temperature-controlled hot air stream in the temperature range of 50 °C to 90 °C for the different samples. The experimental arrangement is shown in Fig. 3. The sample was placed in the center of a Helmholtz coil which generates the magnetic field B_0 in the range of 0.4–1.7 mT for the experiments reported here. Another small coil perpendicular to the B_0 coil was used for the rf pulses. The earth's field was compensated by three pairs of orthogonal Helmholtz coils.

An argon-ion laser (6 W) pumped titanium-sapphire laser (800 mW) served as the optical source. For rubidium atoms the laser was set to 795 nm for optical pumping of the D_1 line. For cesium it was set to 852 nm for optical pumping of the D_2 line. The laser light was split by a beam splitter into a circularly polarized pumping beam (90%) and a weaker linearly polarized probe beam (10%). The pumping light was gated by an acoustic-optic modulator (AOM) and was propagating parallel to the magnetic field B_0. The estimated intensity on the sample was 20 mW/mm^2. The probe light was constantly on and traveled perpendicular to B_0, with its polarization parallel to B_0 (π light). Further attenuation reduced its intensity to less than 1/20 of the pump beam. After traversing the sample cell the light is detected by a polarimeter detector (PD) [18].

The signal received by the polarimeter was mixed with the rf in a double-balanced mixer for phase-coherent quadrature detection (QD) [19]. The signal was further amplified, fed into a boxcar integrator, and stored into a computer. The laser pulse and the three rf pulses of the sequence $(\pi/2)_y$-τ-$(\pi/2)_y$-t_1-$(\pi/2)_y$ were generated by a pulse programmer. Sampling took place at time τ after the third rf pulse. For every increment of the time t_1 one data point is recorded. Increasing t_1 point by point results in the time-domain signal $S(t_1)$. After Fourier transformation of $S(t_1)$, the multiple-quantum spectrum is obtained.

B. Results

In the 1D MQ experiment we have to use an off-resonance technique in order to separate the different MQ spectra. The rf is offset by some 10 kHz with respect to the Larmor frequency. The choice of frequency offset depends on the spectral width of the individual multiple quantum spectra. If the offset is too large, the amplitude of the multiple-quantum lines will become too small. If the offset is too small, all multiple-quantum lines will overlap (see Fig. 5 below). We note moreover that the parameter τ plays an important role. It modulates the amplitude of the n quantum line. The top trace of Fig. 4 shows the 1D MQ spectrum for ^{87}Rb ($F=2$) atoms. The groups of spectral lines appearing along the frequency axis correspond to the nQ transitions of the system.

It is clear that the center frequency of the n quantum (ω_n) transitions is given by $\omega_n = n\Delta\omega$, where $\Delta\omega = \omega_F - \omega_{\rm rf}$ is the frequency offset. The measurements are performed in the rotating frame, where the corresponding Hamilton operator of the Zeeman interaction can be expressed as $H^{(r)} = H_0 - \hbar\omega_{\rm rf} M_F = \hbar\Delta\omega M_F$. According to the Liouville equation

$$\frac{d\rho}{dt} = -i\frac{1}{\hbar}[\rho, H^{(r)}], \tag{14}$$

with

$$\rho = \sum_{k,q} \rho_{kq} T_{kq} \quad \text{and} \quad H^{(r)} = \hbar\Delta\omega T_{10}. \tag{15}$$

From the equation of motion for the multipoles ρ_{kq} it follows immediately that

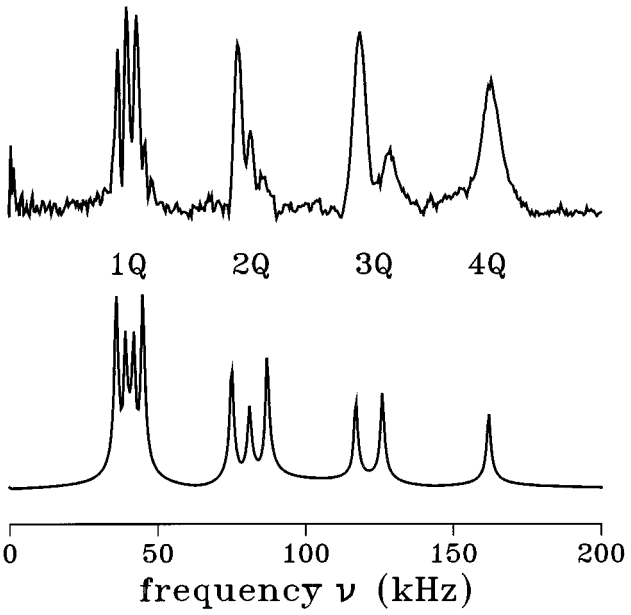

FIG. 4. One-dimensional multiple-quantum spectrum of ^{87}Rb ($F=2$) with large frequency offset ($\Delta\nu = 41$ kHz). Top: experimental (Larmor frequency $\nu_L = 3.029$ MHz), bottom: calculated.

$$\frac{d\rho_{kq}}{dt} = iq\hbar\Delta\omega\rho_{kq} \tag{16}$$

and therefore

$$\rho_{kq} = \rho(0)_{kq} e^{iq\Delta\omega t} = \rho(0)_{kq} e^{i\omega_q t}, \tag{17}$$

leading to a separation of the corresponding multiple-quantum frequencies $\omega_q = q\Delta\omega$ along the offset frequency axis.

Following the derivation of the multiple-quantum spectrum in Sec. II B, we have calculated the 1D MQ spectrum for the ground state of ^{87}Rb atoms ($F=2$). The bottom trace of Fig. 4 shows the calculated spectra. By comparison with the experimental spectra [Fig. 4 (top)] we find good agreement as far as the frequency positions are concerned. We note that the n quantum lines in the calculation are narrower than the experimental ones for $n>1$. The linewidths are determined by the relaxation processes as well as by inhomogeneous magnetic fields B_0. In the calculation we included only a simple relaxation process introduced in Eq. (12) by the time constant T_2. The simulated spectrum was obtained with $T_2 = 300$ μs similar to the experimental result for one-quantum coherences. We note in particular that the linewidth increases with the quantum number n. We will come back to this point later.

For vanishing frequency offset all MQ spectra should overlap in a single spectrum. Using Eq. (3) for spin $F=3$ we calculated the individual nQ-transition frequencies which are shown in Fig. 5(a). Their superposition yields the schematic spectrum shown in Fig. 5(b), where the amplitudes are determined by the number of overlapping lines. For comparison an experimental spectrum [Fig. 5(c)] obtained for ^{133}Cs ($F=3$) is also depicted. Given the experimental results it would not be possible to assign the different quantum orders to the lines in the overlapping MQ spectra without additional

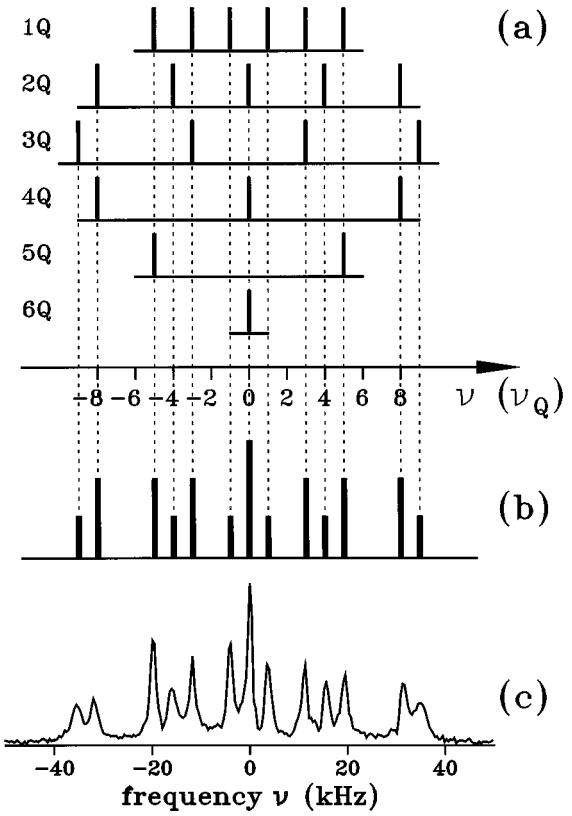

FIG. 5. (a) Theoretical spectral positions of multiple-quantum transitions for $F=3$ according to the Hamiltonian of Eq. (3) ($\Delta\omega=0$). (b) In a 1D experiment the superposition of all individual nQ spectra is observed. (c) Experimental 1D MQ spectrum of the $F=3$ ground state of ^{133}Cs (Larmor frequency $\nu_L=6.044$ MHz). The spectrum shown is the average of three spectra recorded with different values of τ (234, 332, and 408 μs).

information. One possibility to separate the different nQ transitions is to use a frequency offset as discussed above.

IV. TWO-DIMENSIONAL MULTIPLE-QUANTUM SPECTRA

There is a more elegant way of separating MQ spectra than using a frequency offset $\Delta\omega$. This is achieved by using the phase incrementation technique applied already in MQ NMR [1,3,4,20]. It utilizes the rotational property of the n-quantum coherence, namely, that a rotation of an n-quantum coherent state by an angle ϕ around the z axis (by the M_F operator) results in a phase shift of $n\phi$. In order to do so the first two pulses in the three-pulse sequence shown in Fig. 2 are shifted by an angle ϕ with respect to the third pulse. For a fixed value of τ the resulting signal of the detection beam, $S_{2D}(\phi,t_1)$, now depends on both parameters ϕ and t_1. If ϕ is varied in increments as $\phi=2\pi t'/T$ with $0\leqslant t'\leqslant T$, a fictitious time axis t' with fundamental frequency $\Delta\omega=2\pi/T$ is created, which serves as a fictitious frequency offset. The detection signal may now be expressed as $S_{2D}(t',t_1)$ which after a 2D Fourier transformation will result in a 2D MQ spectrum.

We have performed this type of experiment on the spin-polarized ground states of ^{87}Rb ($F=2$), ^{85}Rb ($F=3$), and

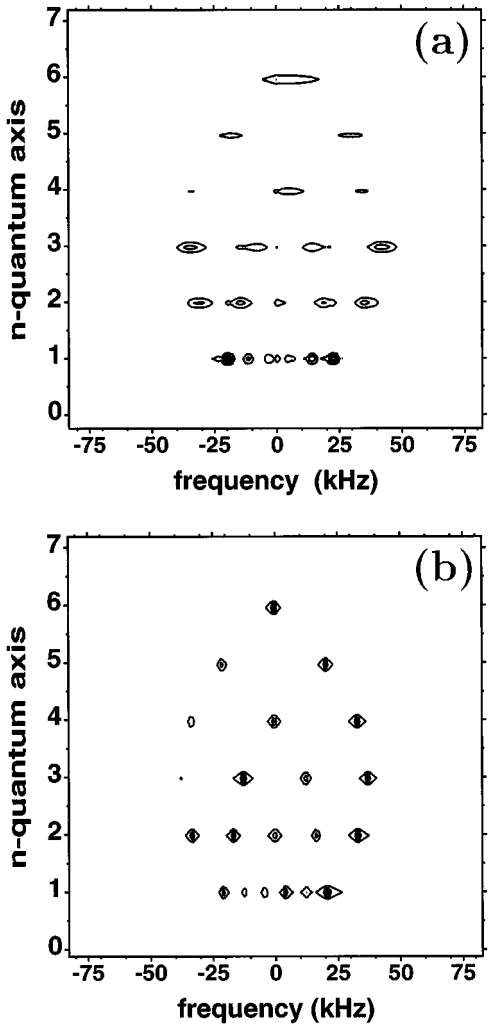

FIG. 6. Experimental (a) and calculated (b) 2D MQ spectra of the $F=3$ ground state of ^{85}Rb, depicted as contour plots. The experimental spectrum is an average of spectra recorded with $\tau=128,144,184$ μs (Larmor frequency $\nu_L=3.5986$ MHz).

^{133}Cs ($F=4$) and representative results for ^{85}Rb and ^{133}Cs are shown in Figs. 6(a) and 7(a), respectively, one as a contour plot, the other as a stacked plot, giving a perspective view of the two-dimensional spectrum.

Since the amplitudes of the MQ lines depend strongly on the value of τ, a τ-ensemble average must be used in order to observe all possible lines.

The n-quantum spectra are nicely separated due to the phase incrementation procedure, as is evident from Figs. 6 and 7. This can be rationalized readily by taking a closer look at the rotational properties of the density matrix in the tensor operator form as used here. We obtain

$$\rho(0)=\sum_{k,q}\rho_{kq}T_{kq},$$

$$\rho(\phi)=e^{-i\phi T_{10}}\sum_{k,q}\rho_{kq}T_{kq}e^{i\phi T_{10}}=\sum_{k,q}\rho_{kq}e^{-iq\phi}T_{kq}. \tag{18}$$

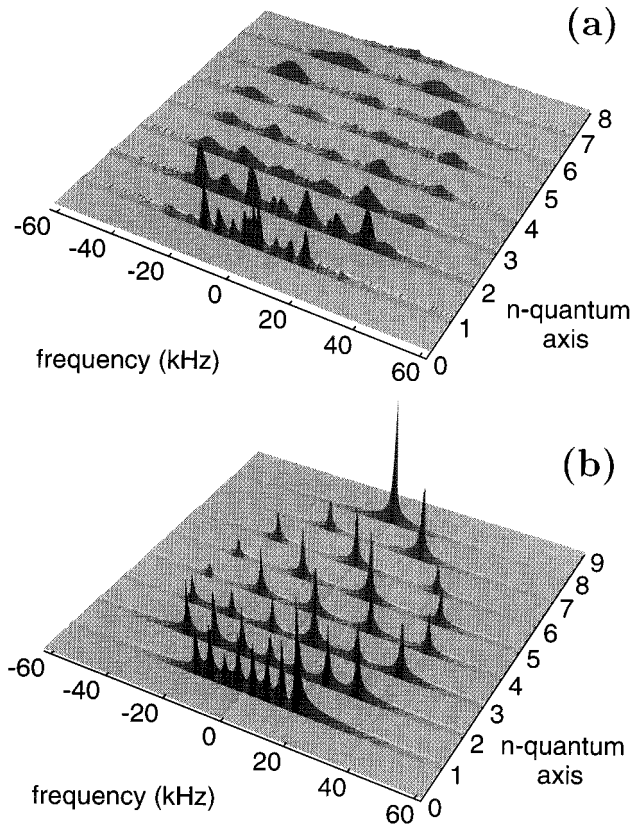

FIG. 7. Experimental (a) 2D MQ spectrum and calculated (b) 2D MQ spectrum of ^{133}Cs ($F=4$), shown as stacked plots. The experimental spectrum is an average of spectra recorded with $\tau=164,182,226$ μs (Larmor frequency $\nu_L=4.6630$ MHz).

The multipole $\rho(\phi)_{kq}=\rho_{kq}e^{-iq\phi}$ contains a phase factor $q\phi$ which directly reflects the separation of the n-quantum spectra.

The calculation of the 2D MQ spectra proceeds along the following lines. Quadrature detection [19] is used resulting in two signals with 90° phase shift between them, which can be expressed as

$$S_{\mathrm{Re}}=\sum_{F_g,F_e}-\frac{\sqrt{2}}{4}iVC_1[T_{S_1}(\phi,\tau,t_1,\tau)e^{-(2\tau+t_1)/T_2}+T_{S_0}(\phi,\tau,\tau)e^{-2\tau/T_2}],$$

$$S_{\mathrm{Im}}=\sum_{F_g,F_e}-\frac{\sqrt{2}}{4}iVC_1[T_{SI_1}(\phi,\tau,t_1,\tau)e^{-(2\tau+t_1)/T_2}+T_{SI_0}(\phi,\tau,\tau)e^{-2\tau/T_2}], \quad (19)$$

where T_{S_0} and T_{S_1} are given by Eqs. (10). The functions T_{SI_0} and T_{SI_1} are abbreviations for

$$T_{SI_0}(\phi,\tau,\tau)=i\cos^2(\omega_F\tau)M_{CPPC}(11,11),$$

$$T_{SI_1}(\phi,\tau,t_1,\tau)=i[\cos^2(\omega_F\tau)M_{CPCPC}(gc,11)-\sin^2(\omega_F\tau)M_{CPCPC}(uc,11)]. \quad (20)$$

In the complex signal

$$S_{2D}(\phi,t_1)=S_{\mathrm{Re}}+iS_{\mathrm{Im}} \quad (21)$$

both quadrature signals have been combined. After 2D Fourier transformation, the 2D MQ spectrum results,

$$F_{2D}(n,\omega)=\int_0^\infty d\phi\ \exp(-iAn\phi)\times\int_0^\infty dt_1\exp(-i\omega t_1)S_{2D}(\phi,t_1), \quad (22)$$

where n is the quantum number and A a scale factor. It is evident from this, that one axis of the 2D function F_{2D} represents the n quantum axis, whereas the other one is the ω axis corresponding to the time scale of t_1.

Using Eq. (22) and reasonable parameters reflecting the experimental situation, we have calculated the corresponding 2D MQ spectra. The calculated 2D MQ spectra are shown in Fig. 6(b) (contour plot) and Fig. 7 (3D rendering) together with the experimental spectra.

The agreement between the experimental and theoretical spectra is very satisfactory as far as the overall structure and line positions are concerned. The experimental linewidth of n-quantum spectra, however, appears to increase with quantum number n, which is not reflected in the simulations. The reason for this is the assumption of only a single dephasing relaxation time T_2, independent of the quantum number n in the calculations.

The decoherence processes in multiple-quantum coherence spectroscopy are rather involved if one goes beyond simple field-inhomogeneity effects. They have some relevance to the decoherence of entangled (Schrödinger cat) states as is discussed by Goetsch *et al.* [21]. Our contribution is mainly concerned with multiple-quantum coherence phenomena rather than with decoherence processes. Nevertheless, we want to point out that we observe a monotonic increase of decoherence with increasing order of multiple quantum coherence as is expected for Schrödinger cat states [21]. This increase can, however, partially be rationalized on the simple physical ground that a fluctuation of the hyperfine interaction caused by atomic collisions with the walls or among each other results in level-shift differences which can be expressed in the form $\Delta E_n=an+bn^2$, where n labels the n-quantum coherence. Since in the rapid motion limit the square of this energy difference enters the relaxation expressions, the decoherence rapidly increases with increasing quantum order n. Details can readily be worked out, but are not the topic of this contribution.

Finally we want to point out an artifact in the 1Q spectrum of Figs. 6(a) and 7(a), where an additional (unexpected) line appears in the middle of the spectra. It arises from an incomplete separation of the 1Q and 2Q spectra due to phase errors during detection time. Clearly such artifacts are not present in the theoretical spectra.

V. CONCLUSION

We have demonstrated the creation and detection of multiple-quantum coherences in the ground state of alkali atomic vapors. All possible multiple-quantum coherences for a given F-spin multiplet up to the $2F$-quantum coherence

have been observed. The individual nQ spectra can be fully explained by using only a Zeeman term ($\sim M_F$) and a pseudo-quadrupolar term ($\sim M_F^2$) in the magnetic field range studied here. The linewidth or the corresponding dephasing rate is observed to increase with quantum number n. Much larger fields would lead to higher order tensor operators T_{k0} with $k>2$ in the Hamiltonian of Eq. (3). This would still result in the same multiple-quantum coherences as discussed here, however, the current treatment must be extended in this case and would lead to different intensities of the observed multiple quantum lines.

Finally we want to stress that the excitation and detection of the multiple-quantum coherence can be performed by virtue of the concerted action of the rf-pulse operation which changes the quantum number q but keeps the rank k of the tensor operator T_{kq} constant, whereas the evolution under the action of the pseudoquadrupolar Hamiltonian does the opposite. The separation of the nQ spectra was achieved either by frequency offset $\Delta\omega$ or by phase incrementing ($\Delta\phi$) the first two pulses in the three-pulse sequence, in the latter case rendering a two-dimensional spectrum, where the different quantum orders are separated along the additional axis.

ACKNOWLEDGMENT

We gratefully acknowledge financial support by the Deutsche Forschungsgemeinschaft (SFB 228-B3).

[1] M. Mehring, *Principles of High Resolution NMR in Solids* (Springer, Berlin, 1983).
[2] D. P. Weitekamp, Adv. Magn. Res. **11**, 111 (1983).
[3] M. Munowitz and A. Pines, Adv. Chem. Phys. **66**, 1 (1987).
[4] R. R. Ernst, G. Bodenhausen, and A. Wokaun, *Principles of Nuclear Magnetic Resonance in One and Two Dimensions* (Clarendon Press, Oxford, 1987).
[5] M. Goeppert-Mayer, Ann. Phys. (Leipzig) **9**, 273 (1931).
[6] J. M. Winter, Ann. Phys. (Paris) **4**, 745 (1959).
[7] E. Arimondo and R. Corbalan, J. Phys. B **7**, 2368 (1974); E. Arimondo and G. Moruzzi, *ibid.* **9**, 709 (1976); **9**, 723 (1976).
[8] M. Munowitz and A. Pines, Adv. Chem. Phys. **66**, 1 (1987).
[9] W. S. Warren, D. P. Weitekamp, and A. Pines, J. Chem. Phys. **73**, 2084 (1980).
[10] B. C. Sanctuary and T. K. Halstead, Adv. Magn. Opt. Res. **15**, 79 (1990).
[11] G. J. Bowden and W. D. Hutchison, J. Magn. Res. **67**, 403 (1986).
[12] G. J. Bowden, W. D. Hutchison, and J. Khachan, J. Magn. Res. **67**, 415 (1986).
[13] W. Happer, Rev. Mod. Phys. **44**, 169 (1972).
[14] A. Omont, Prog. Quantum Electron. **5**, 69 (1977).
[15] G. Breit and I. I. Rabi, Phys. Rev. **38**, 2082 (1931).
[16] C. Cohen-Tannoudji and F. Laloë, J. Phys. (Paris) **28**, 505 (1967); **28**, 722 (1967).
[17] J. D. Xu, Ph. D. thesis, Universität Stuttgart, 1996.
[18] G. Wäckerle, St. Appelt, and M. Mehring, Phys. Rev. A **43**, 242 (1991).
[19] D. I. Hoult, Prog. Nucl. Magn. Reson. Spectrosc. **12**, 41 (1978).
[20] G. Drobny *et al.*, Symp. Faraday Soc. **13**, 49 (1979).
[21] P. Goetsch, R. Graham, and F. Haake, Phys. Rev. A **51**, 136 (1995); Quantum Semiclass. Opt. **8**, 157 (1996).